HYBRID METHODS: THE GENERALIZAED INTEGRAL TRANSFORM TECHNIQUE

Renato M. Cotta
Laboratory of Transmission and Technology of Heat
Mechanical Engineering Dept. – EE/COPPE – UFRJ
Universidade Federal do Rio de Janeiro
Cx. Postal 68503 – Rio de Janeiro, RJ 21945-970, Brazil
E-mail: cotta@serv.com.ufrj.br

1. INTRODUCTION

Around the turn of the 19th century and along the first half of the 20th century, different analytical approaches were devised for solving partial differential equations that model various engineering applications. Although severely limited to certain classes of problems, almost always as linear or linearized formulations, these classical ideas were responsible for a considerable amount of mathematical and physical analysis, that markedly aided the technological progress then achieved, supporting the intense experimental activity still required. The second half of this century, due to the increasing availability of computational performance, after both the hardware enhancement and numerical methods development, witnessed the

continuous advancement of the role of computational simulation in engineering analysis and design. Discrete numerical methods are still nowadays responsible for most of the challenges and tasks accomplished, and most frequently employed in commercial software for multipurpose usage. Nevertheless, a number of hybrid methodologies have been appearing in the open literature, that to within different degrees of success, attempt to match the classical analytical ideas with the presently solid knowledge basis on numerical analysis.

Within the last two decades, the classical integral transform method [1] gained a hybrid numerical-analytical structure, offering user controlled accuracy and quite efficient computational performance for a wide variety of *a priori* non transformable problems [2-6], including the nonlinear formulations of interest in heat and fluid flow applications. Besides being an alternative computational method on itself, this hybrid approach is particularly well suited for benchmarking purposes, in light of its automatic error control feature, retaining the same characteristics of a purely analytical solution. In addition to the straightforward error control and estimation, an outstanding aspect of this method is the direct extension to multidimensional situations, with a moderate increase in computational effort with respect to one-dimensional applications. Again, the hybrid nature is responsible for this behavior, since the analytical part in the solution procedure is employed over all but one independent variable, and the numerical task is always reduced to the integration of an ordinary differential system in this one single independent variable.

The present chapter reviews the concepts behind the Generalized Integral Transform Technique (GITT), as an example of a hybrid method in heat transfer applications, which adds to the available simulation tools, either as a companion in covalidation tasks or as an alternative approach for analytically oriented users.

2. FORMAL SOLUTION

As an illustration of the formal solution procedure, we consider here a transient convection-diffusion problem of n coupled potentials (velocity, temperature or concentration), defined in the region V with boundary surface S, and including non-linear effects in the convective terms as follows:

$$w_k(\boldsymbol{x})\frac{\partial T_k(\boldsymbol{x},t)}{\partial t}+\boldsymbol{u}(\boldsymbol{x},t,T_\ell).\nabla T_k(\boldsymbol{x},t)+LT_k(\boldsymbol{x},t)=P_k(\boldsymbol{x},t,T_k),$$

$$\boldsymbol{x}\in V,\quad t>0,\quad k,\ell=1,2,...,n \tag{1.a}$$

with initial and boundary conditions given, respectively, by

$$T_k(\boldsymbol{x},0)=f_k(\boldsymbol{x}),\qquad \boldsymbol{x}\in V \tag{1.b}$$

$$\left[\alpha_k(\boldsymbol{x})+\beta_k(\boldsymbol{x})k_k(\boldsymbol{x})\frac{\partial}{\partial \boldsymbol{n}}\right]T_k(\boldsymbol{x},t)=\phi_k(\boldsymbol{x},t,T_k), \tag{1.c}$$

$$\boldsymbol{x}\in S,\quad t>0$$

where the equation operator is written as:

$$L_k\equiv-\nabla k_k(\boldsymbol{x})\nabla+d_k(\boldsymbol{x}) \tag{1.d}$$

and $\boldsymbol{n}$ denotes the outward drawn normal to the surface S.

Without the convection terms and for linear source terms, i.e. $\boldsymbol{u}(\boldsymbol{x}, t, T_\ell) \equiv 0$, $P\equiv P(\boldsymbol{x},t)$, and $\phi\equiv\phi(\boldsymbol{x},t)$, problem (1) becomes a class I linear diffusion problem according to an earlier classification [1], for which exact

analytical solutions were obtained through the classical integral transform technique. Otherwise, problem (1) is not *a priori* transformable, and the ideas in the generalized integral transform technique [2-6] can be utilized to develop hybrid numerical-analytical solutions to this class of problems. Following the formalism previously established for convection-diffusion and purely diffusive non-linear problems [7-8], the appropriate auxiliary problems are taken as:

$$L_k\psi_{ki}(\boldsymbol{x}) = \mu_{ki}^2 w_k(\boldsymbol{x})\psi_{ki}(\boldsymbol{x}), \qquad \boldsymbol{x} \in V \tag{2.a}$$

with boundary conditions

$$\left[\alpha_k(\boldsymbol{x}) + \beta_k(\boldsymbol{x})k_k(\boldsymbol{x})\frac{\partial}{\partial \boldsymbol{n}}\right]\psi_{ki}(\boldsymbol{x}) = 0, \qquad \boldsymbol{x} \in S \tag{2.b}$$

where the eigenvalues, $\mu_{ki}{}'s$, and related eigenfunctions, $\psi_{ki}(\boldsymbol{x})$, are here assumed to be known from application of also recently advanced computational methods for Sturm-Liouville type problems [1,2]. Problem (2) then allows, through the associated orthogonality property of the eigenfunctions, definition of the integral transform pairs below:

$$\overline{T}_{k,i}(t) = \int_V w_k(\boldsymbol{x})K_{ki}(\boldsymbol{x})T_k(\boldsymbol{x},t)dv, \text{ transforms} \tag{3.a}$$

$$T_k(\boldsymbol{x},t) = \sum_{i=1}^{\infty} K_{ki}(\boldsymbol{x})\overline{T}_{k,i}(t), \text{ inverses} \tag{3.b}$$

where the symmetric kernels $K_{ki}(\boldsymbol{x})$ are given by:

$$K_{ki}(\boldsymbol{x}) = \frac{\psi_{ki}(\boldsymbol{x})}{N_{ki}^{1/2}} \quad ; \qquad N_{ki} = \int_v w_k(\boldsymbol{x})\psi_{ki}^2(\boldsymbol{x})dv \tag{3.c,d}$$

The integral transformation of (1.a) is now accomplished by applying the operator $\int_v K_{ki}(\boldsymbol{x})dv$ to yield, after using boundary conditions (1.c, 2.b):

$$\frac{d\overline{T}_{k,i}(t)}{dt} + \sum_{j=1}^{\infty} a_{kij}(t,T_\ell)\overline{T}_{k,j}(t) = \overline{g}_{ki}(t,T_k), \qquad i = 1,2,\ldots, \qquad t > 0,$$

$$k,\ell = 1,2,\ldots,n \tag{4.a}$$

The initial conditions (1.b) are also integral transformed through the operator $\int_v w_k(\boldsymbol{x})K_{ki}(\boldsymbol{x})dv$, to provide:

$$\overline{T}_{k,i}(0) = \bar{f}_{ki} \equiv \int_v w_k(\boldsymbol{x})K_{ki}(\boldsymbol{x})f_k(\boldsymbol{x})dv \tag{4.b}$$

where,

$$\overline{g}_{ki}(t,T_k) = \int_v \mathrm{K_{ki}}(\boldsymbol{x})P_k(\boldsymbol{x},t,T_k)dv + \int_S \mathrm{k_k}(\boldsymbol{x})$$

$$\left[\mathrm{K_{ki}}(\boldsymbol{x})\frac{\partial T_k(\boldsymbol{x},t)}{\partial \boldsymbol{n}} - T_{\mathrm{k}}(\boldsymbol{x},t)\frac{\partial K_{ki}(\boldsymbol{x})}{\partial \boldsymbol{n}}\right]\mathrm{ds}$$

(4.c)

$$a_{kij}(t,T_f) = \delta_{ij}\mu_{ki}^2 + a_{kij}^{*}(t,T_f) \tag{4.d}$$

with

$$\delta_{ij} = \begin{cases} 0, & for \quad i \neq j \\ 1, & for \quad i = j \end{cases} \tag{4.e}$$

$$a_{kij}^{*}(t,T_f) = \int_v K_{ki}(\boldsymbol{x})[\boldsymbol{u}(\boldsymbol{x},t,T_f).\nabla K_{ki}(\boldsymbol{x})]dv \tag{4.f}$$

Equations (4) form an infinite system of coupled non-linear ordinary differential equations for the transformed potentials, $\overline{T}_{k,i}{}'s$. For computation purposes, system (4) is truncated at the Nth row and column, with N sufficiently large for the required convergence. The formal aspects behind the convergence to the infinite system solution as the truncation order, N, is increased, have been investigated in [2]. The non-linear initial value problem defined by eqs. (4) is likely to belong to a class of stiff ordinary differential systems, especially for increasing values of N. Fortunately, various special numerical integrators have been designed within the last two decades, to this class of systems[9]. Once the transformed potentials have been computed from numerical solution of system (4), the inversion formula (3b) is recalled to reconstruct the original potentials $T_k(\boldsymbol{x},t)$, in explicit form.

3. COMPUTATIONAL PROCEDURE

A quite straightforward algorithm can be constructed as follows:

- The auxiliary eigenvalue problem is solved for the eigenvalues and related normalized eigenfunctions, either in analytic form when applicable or through the GITT itself [1,2].
- The transformed initial or boundary conditions are computed, either analytically or, in a general-purpose procedure, through adaptive numerical integration[9]. Similarly, those coefficients on the transformed O.D.E. system, which are not dependent on the transformed potentials, can be evaluated a *priori*. For nonlinear coefficients, there are some computational savings in grouping them into a single integrand.
- The truncated O.D.E. system in then numerically solved through different tools, depending on the type of problem under consideration. For an initial value problem, the numerical integration is performed, for instance, through subroutine DIVPAG[9], since the resulting system is likely to become stiff, especially for increasing truncation orders. Boundary value problems can be handled through subroutine DBVPFD[9], an adaptive finite-difference program for first order nonlinear boundary value problems. Both subroutines offer an interesting combination of accuracy control, simplicity in use and reliability.

Since all the intermediate numerical tasks are accomplished within user prescribed accuracy, one is left with the need of reaching convergence in the eigenfunction expansions and automatically controlling the truncation order N, for the requested accuracy in the final solution. The analytic nature of the inversion formulae allows for a direct testing procedure at each specified position within the medium where a solution is desired, and the truncation order N can be gradually decreased (or eventually increased), to fit the user global error requirements over all the solution domain.

The simple tolerance testing formula employed is written as:

$$\varepsilon = \max_{x \in V} \left| \frac{\sum_{i=N^*}^{N} \tilde{\psi}_i(x) \overline{T}_i(t)}{T_s(x;t) + \sum_{i=1}^{N} \tilde{\psi}_i(x) \overline{T}_i(t)} \right| \tag{5}$$

where T_s is a filtering solution, if eventually employed, and N^* is decreased from the value of N while ε still fits the user requested global error, and then N is changed to assume the value of N^*.

4. FILTERING AND REORDERING STRATEGIES

A major aspect in the practical implementation of this methodology is the eventual need for improving the convergence behavior of the resulting eigenfunction expansions. Within the context of those classes of problems that may be handled exactly, convergence acceleration schemes were proposed [1], essentially originated from the splitting-up of the original partial differential system into simpler problems. However, the expressions so developed are limited to special linear cases. Motivated by the developments in the GITT, an alternative approach based on integral balances was proposed and different filtering schemes were employed throughout the sparse literature on this methodology [2]. The aim was to provide simpler convergence enhancement procedures, in order to maintain the applicability of the formal solution approach into the widest possible range of proposed problems in heat and fluid flow, and to within a mild degree of analytical involvement, for compatibility with the development of automatic solvers for

partial differential equations in such fields. More recently [10], these ideas were more closely examined and different convergence improvement strategies were critically compared. While multiple successive filtering proved to be the most efficient computationally, it was also demonstrated to become progressively quite too involved for practical purposes, and not necessarily uniformly effective over the whole solution domain.

One possible alternative for further improvement appears to be the proposition of analytical filtering solutions, which present both space and time dependence, within ranges of the time numerical integration path. For instance, representative linearized versions of the original problem in a certain time interval, after being exactly solved through the classical integral transform approach, may more effectively partially filter the original problem source terms, which are responsible for deviating the convergence behavior from the spectral exponential pattern. Then, the filter can be automatically redefined for the next time variable range, by prescribing a desirable maximum value for the system truncation order, while still satisfying the user requested global accuracy target. This so-called local-instantaneous filtering (L.I.F.) strategy is therefore now preferred, as a possibly optimum scheme, and still user-controllable, for enhancing convergence in eigenfunction expansions [11]. Also, the L.I.F. strategy indirectly introduces a quite desirable modulation effect on the transformed ODE system. While the single filter solution produces, in general, strongly stiff ODE systems, requiring special initial value problem solvers, the L.I.F. solution yields, in principle, non-stiff systems, which are readily solvable by standard explicit schemes at much less computational cost.

In multidimensional applications, the final integral transform solution for the related potential is expressed as double or triple infinite summations for two or three-dimensional transient problems, or a double summation for a three- dimensional steady problem. Each of these

summations is associated with the eigenfunction expansion in a corresponding spatial coordinate, eliminated through integral transformation from the partial differential system, and recovered analytically through such expressions. From a computational point of view, only a truncated version of such nested summations can be actually evaluated. However, the plain truncation of these series, individually, to a certain prescribed finite order, is certainly not an efficient approach and, to an extent, even a risky one. In this way, some still important information to the final result can be disregarded, while other terms are accounted for that have essentially no contribution to convergence in the relative accuracy required. Therefore, for an efficient computation of these expansions, the infinite multiple summations should first be converted to a single sum representation, with the appropriate reordering of terms, according to their individual contribution to the final numerical result. Then, one would be able to evaluate a minimum number of eigenvalues and related derived quantities, as many as required to reach the user prescribed accuracy target. This aspect is even more evident in the use of the GITT, when the computational costs can be markedly reduced through this reordering of terms, which then represents a reduction on the number of ordinary differential equations to be solved numerically in the transformed system [10]. Since the final solution is not, of course, known a priori, the parameter which shall govern this reordering scheme must be chosen with care, and proved to be a good choice. Once the ordering is completed, the remaining of the computational procedure becomes as straightforward and cost-effective as in the one-dimensional case. In fact, except for the additional effort in the evaluation of double and/or triple integrals, when required to be numerically computed, finding a multidimensional solution requires essentially the same order of CPU time as in a plain one-dimensional situation. It is noticeable that the most common choice of ordering strategy, based on the argument of the dominating exponential term,

although not always in a monotonic fashion, offers a good compromise between the overall convergence enhancement and simplicity in use. However, individual applications may require more elaborate reordering that accounts for the influence of nonlinear source terms in the ODE system, for instance based on local linearization and dynamic reordering along the time integration marching.

5. APPLICATIONS

The potential of the integral transform approach in dealing with different classes of nonlinear problems in heat transfer is now briefly illustrated. The examples selected include diffusion in irregular geometries [12-18], here related to fin calculations, diffusion with coupled equations [19-24], as formulated by the Luikov equations of drying, convection-diffusion in the boundary layer formulation [25-29], demonstrated with a mixed convection example, and convection-diffusion in the full Navier-Stokes formulation [30-40], represented by natural convection in enclosures. Additional details on the application of the method can be readily obtained from the original papers that correspond to these topics, and/or from the compilations in [2,10], where several other topics not presented here are also discussed.

5.1 Diffusion:- Irregular Geometries

We consider the two-dimensional heat conduction equation, for steady-state and temperature-dependent thermal conductivity, written for a longitudinal fin of variable profile, according to Fig. 1. The temperature at the fin base is assumed uniform and heat losses through the fin tip are disregarded. In dimensionless form, the problem formulation is given as [12]:

$$\frac{\partial}{\partial Y}\left[K(\theta)\frac{\partial\theta(X,Y)}{\partial Y}\right]+\frac{\partial}{\partial X}\left[K(\theta)\frac{\partial\theta(X,Y)}{\partial X}\right]=0, \qquad (6.a)$$
$$0<X<C, 0<Y<\in(X)$$

with boundary conditions

$$\theta(0,Y)=1; \quad \left.\frac{\partial\theta(X,Y)}{\partial X}\right|_{X=C}=0 \qquad (6.b,c)$$

$$\left.\frac{\partial\theta(X,Y)}{\partial Y}\right|_{Y=0}=0; \left[K(\theta)\left(sin\alpha\frac{\partial\theta}{\partial X}+\cos\alpha\frac{\partial\theta}{\partial Y}\right)\right]_{Y=\in(X)}$$
$$+Bi\theta(X,\in(X))=0 \qquad (6.d,e)$$

where the various dimensionless groups are defined by

$$X=\frac{x}{\varepsilon_o}; Y=\frac{y}{\varepsilon_o}; \theta(X,Y)=\frac{T(x,y)-T_\infty}{T_b-T_\infty}$$

$$C=\frac{L}{\varepsilon_o}; Bi=\frac{h\varepsilon_o}{k_\infty}; K(\theta)=\frac{k(T)}{k_\infty} \qquad (7)$$

and α is the local inclination of the variable profile.

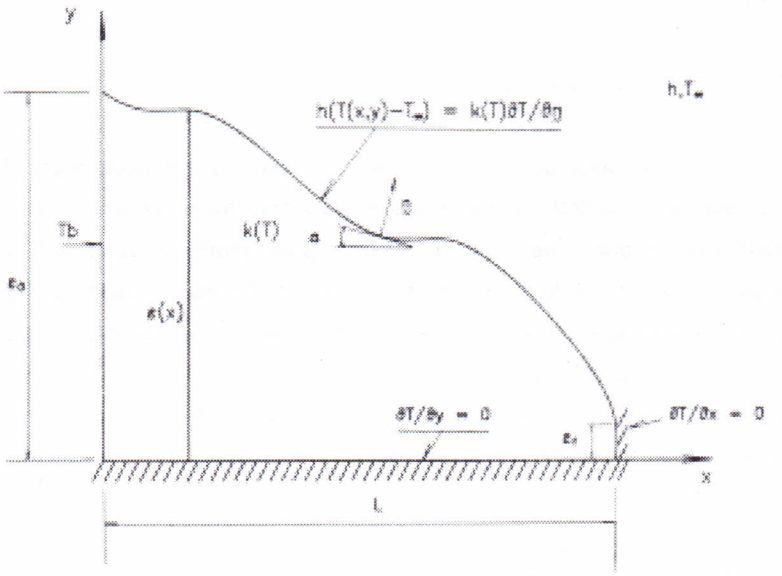

Figure 1. Geometry and coordinate system for a longitudinal fin with variable profile

If the temperature-dependent thermal conductivity is considered in the usual linear form

$$k(T) = k_{\infty} [1 + \beta(T - T_{\infty})] \tag{8.a}$$

in order to reduce the number of parameters to be studied, then the dimensionless function $K(\theta)$ becomes

$$K(\theta) = 1 + b\theta \tag{8.b}$$

where,

$$b = \beta(T_b - T_\infty) \tag{8.c}$$

Results are then obtained for the present application. The automatic error control feature of the integral transform approach was first reconfirmed through the case of a rectangular profile ($\epsilon(X)=const.$) and constant thermal conductivity, which has a straightforward exact analytical solution. As expected, the agreement was perfect to within the requested relative error target (10^{-5}).

Next, the case of a trapezoidal profile with constant thermal conductivity was considered, which is represented by the following equation

$$\epsilon(X) = 1 + \frac{X}{C}(r-1) \tag{9.a}$$

where,

$$r = \frac{\varepsilon_f}{\varepsilon_o}; \tan\alpha = \frac{1-r}{C} \tag{9.b,c}$$

The special case of a triangular fin [17] is then recovered by letting $r \to 0$.

Table 1 illustrates the convergence behavior of the proposed eigenfunction expansion for the average temperature, in the case of a trapezoidal fin of constant thermal conductivity for different values of Biot number, *Bi*, and aspect ratio, *C*. Also shown are the results from the classical

one-dimensional formulation for a trapezoidal fin [18]. It is clearly noticeable that the convergence rates are somehow improved for lower values of *Bi* and higher values of *C*, since then the *X*-component of the boundary normal derivative becomes less significant. This component is not incorporated in the eigenvalue problem boundary condition, and appears as a "source term" in the system for the transformed potential, therefore affecting the convergence rates, as usual in eigenfunction expansion-type approaches. However, the overall convergence behavior is still quite outstanding, at least in the range of the parameters, typical of extended surfaces applications, here considered. When required, convergence acceleration schemes can be recalled, either through filtering solutions or integral balance procedures, with additional analytical involvement. The results presented in Table 1 are achieved through an user prescribed accuracy of 10^{-5} in the ODEs solver.

Table 1 also presents the classical one-dimensional fin formulation [18], compared with the full two-dimensional formulation here obtained. As expected, the error increases with the Biot number, as the temperature gradients in the transversal direction become more pronounced. It is also of interest to observe the behavior of the two-dimensional solution with one single term in the eigenfunction expansion (N=1). From the mathematical point of view, this solution is as simple as the classical one-dimensional formulation, i.e. it is obtained essentially from the solution of a single second order ordinary differential equation. Nevertheless, the error for this alternative approximate solution (N=1) is better behaved than that for the classical one-dimensional solution. This behavior is even more noticeable for higher values of *Bi* (=1.0) and/or *C* (=10.0), indicating that in the realm of applications and for optimization studies of reduced cost, this approximate solution might offer a more reliable alternative to the classical approach.

Such aspects of convergence rates and relative accuracy are also observable in graphical form, through Fig. 2, for the average temperature distribution along the entire length of the fin. Fig. 2 shows the convergence behavior for the case C=3.0 and Bi=0.1, demonstrating the practically coincident results, to the graph scale, for $N \geq 4$. In addition, the results for one single term in the expansion (N=1) are in very good agreement with the one-dimensional solution, over the whole domain. Results were also obtained for a longitudinal fin with concave parabolic profile, again for constant thermal conductivity, defined by the following expression:

$$\in (X) = \left(\frac{X}{C} - 1 \right)^2 \tag{10}$$

In reference [1], the classical one-dimensional formulation was employed in the solution of concave parabolic fins with negligible thickness at the fin tip. In order to allow for critical comparisons with the present two-dimensional results, the computations were performed with $r=10^{-5}$, which was verified to represent adequately the situation of $r \rightarrow 0$, or negligible heat transfer area at the tip. Numerical results are then presented in graphical form, to illustrate both the convergence rates and relative accuracy of the approximate solutions in the case of a parabolic profile. Fig. 3 shows the convergence of the eigenfunction expansion for the average temperature along the fin length, together with the approximate one-dimensional solutions with C=3.0 and Bi=0.1. The same trends observed for the trapezoidal profile are present in these comparisons for the parabolic geometry.

Table 1. Convergence of the eigenfunction expansion and comparison with the classical one-dimensional formulation (C=3.0; r=10^{-3}; b=0 - trapezoidal fin)

N	Bi = 1.00			
	X=0.0	X=0.750	X =1.875	X =3.0
1	1.0	0.5144	0.1483	0.0185
% error		(1.672)	(3.974)	(9.445)
4	1.0	0.5067	0.1431	0.0171
7	1.0	0.5062	0.1428	0.0170
10	1.0	0.5060	0.1427	0.0169
(*)	1.0	0.4726	0.1195	0.0134
% error		(7.073)	(19.38)	(24.42)
N	Bi = 0.10			
	X =0.0	X =0.750	X =1.875	X =3.0
1	1.0	0.8465	0.6401	0.4711
% error		(0.497)	(1.303)	(2.353)
4	1.0	0.8427	0.6357	0.4615
7	1.0	0.8424	0.6350	0.4606
10	1.0	0.8423	0.6348	0.4603
(*)	1.0	0.8407	0.6316	0.4571
% error		(0.189)	(0.508)	(0.696)
N	Bi = 0.01			
	X=0.0	X=0.750	X=1.875	X=3.0
1	1.0	0.9783	0.9462	0.9151
% error		(0.077)	(0.194)	(0.312)
4	1.0	0.9776	0.9446	0.9126
7	1.0	0.9776	0.9444	0.9123
10	1.0	0.9775	0.9444	0.9122
(*)	1.0	0.9775	0.9442	0.9120
% error		(0.005)	(0.019)	(0.027)

Attention is now directed to the solution of the nonlinear situation due to a temperature dependent thermal conductivity, for different values of the governing coefficient, b. Table 2 illustrates the convergence rates of the eigenfunction expansion for a trapezoidal fin with variable thermal conductivity, with Bi=0.1, C=10 and b=0.01, 0.1, 1.0.

The average temperature results are in all cases fully converged to four digits with N as low as 4. Also shown are the results for the one-dimensional formulation, when the average value of the dimensionless thermal conductivity is adopted (K_{av}=1+b/2), in the temperature range of the problem. Clearly, the results from the single-term eigenfunction expansion (N=1), offer an excellent approximation of the two-dimensional formulation, with considerable accuracy improvement over the classical one-dimensional approach, and even more noticeably for an increasing degree of nonlinearity.

Table 1 (cont.) (C=10; r=10^{-3}; b=0 - trapezoidal fin)

N	Bi = 1.00			
	X=0.0	X=3.750	X=6.250	X=10.0
1	1.0	0.0267	0.0011	0.0000
% error		(0.755)	(0.000)	(0.000)
4	1.0	0.0264	0.0011	0.0000
7	1.0	0.0265	0.0011	0.0000
10	1.0	0.0265	0.0011	0.0000
(*)	1.0	0.0169	0.0005	0.0000
% error	-	(-36.62)	(-51.01)	(-89.94)
N	Bi = 0.10			
	X=0.0	X=3.750	X=6.250	X=10.0
1	1.0	0.3052	0.1143	0.0118
% error		(0.246)	(0.422)	(0.943)
4	1.0	0.3045	0.1138	0.0117
7	1.0	0.3044	0.1138	0.0117
10	1.0	0.3044	0.1138	0.0117
(*)	1.0	0.3001	0.1113	0.0113
% error		(-1.668)	(-2.584)	(-3.683)
N	Bi = 0.01			
	X=0.0	X=3.750	X=6.250	X=10.0
1	1.0	0.7588	0.6193	0.4408
% error		(0.068)	(0.121)	(0.220)
4	1.0	0.7583	0.6186	0.4408
7	1.0	0.7583	0.6185	0.4399
10	1.0	0.7583	0.6185	0.4398
(*)	1.0	0.7580	0.6182	0.4395
% error		(-0.039)	(-0.048)	(-0.068)

(*) One-dimensional solution [18]

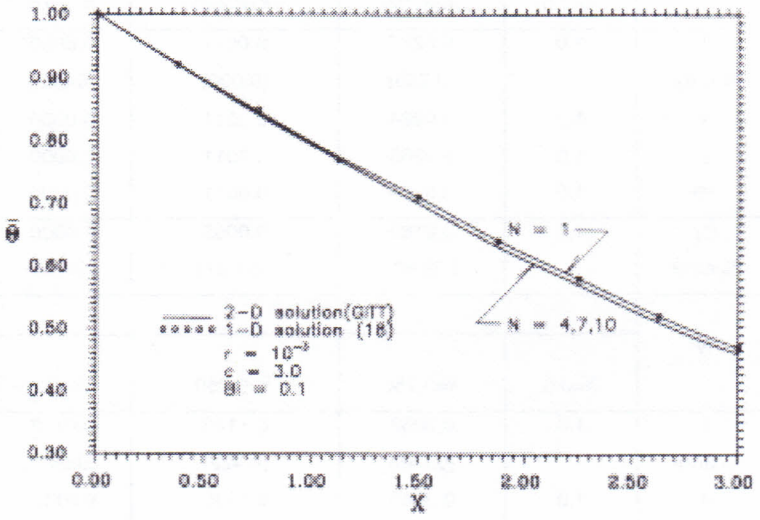

Figure 2: Convergence of the integral transform solution for a trapezoidal longitudinal fin

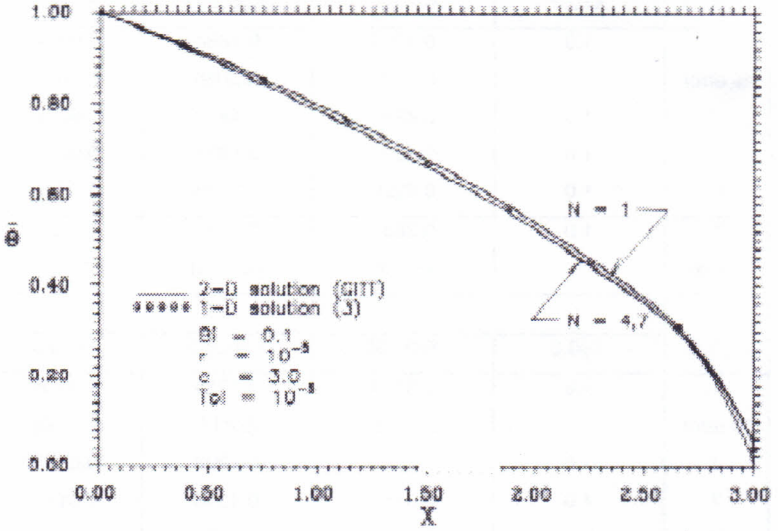

Figure 3: Convergence of the integral transform solution for a concave parabolic fin

Table 2: Convergence of the eigenfunction expansion for a trapezoidal fin with variable thermal conductivity ($Bi = 0.10$; $C = 10.0$; $r = 10^{-3}$)

	$b = 1.0$			
N	X=0.0	X=3.750	X=6.250	X=10.0
1	1.0	0.4295	0.1884	0.0219
% error		(0.116)	(0.319)	(0.922)
4	1.0	0.4290	0.1879	0.0218
7	1.0	0.4290	0.1878	0.0217
10	1.0	0.4290	0.1878	0.0217
(*)	1.0	0.3837	0.1758	0.0322
% error		(-10.56)	(-6.390)	(48.37)
	$b = 0.1$			
N	X=0.0	X=3.750	X=6.250	X=10.0
1	1.0	0.3194	0.1213	0.0126
% error		(0.220)	(0.414)	(0.800)
4	1.0	0.3187	0.1208	0.0125
7	1.0	0.3187	0.1208	0.0125
10	1.0	0.3187	0.1208	0.0125
(*)	1.0	0.3099	0.1182	0.0130
% error		(-2.761)	(-2.152)	(4.000)
	$b = 0.01$			
N	X=0.0	X=3.750	X=6.250	X=10.0
1	1.0	0.3066	0.1150	0.0119
% error		(0.229)	(0.437)	(0.847)
4	1.0	0.3059	0.1145	0.0118
7	1.0	0.3059	0.1145	0.0118
10	1.0	0.3059	0.1145	0.0118
(*)	1.0	0.3011	0.1120	0.0115
% error		(-1.569)	(-2.183)	(-2.542)

(*) One-dimensional linearized solution for K_{av}

5.2 Diffusion:- Coupled Equations

The approach here reviewed is now illustrated for simultaneous heat and mass diffusion within a porous moist sheet, undergoing drying through one boundary (or both) subjected to coupled convective-radiative heat exchange with the environment. In order to reduce the number of parameters to be studied, the assumption of constant transport coefficients is adopted, and the nonlinear behavior is restricted to the radiation boundary condition [23]. Recalling the system of equations proposed by Luikov [19], the problem formulation in dimensionless form is written as [22]:

$$\frac{\partial \theta_1(X,\tau)}{\partial \tau} = \frac{\partial^2 \theta_1(X,\tau)}{\partial X^2} - \varepsilon Ko \frac{\partial \theta_2(X,\tau)}{\partial \tau}, \qquad 0 < X < 1, \quad \tau > 0 \tag{11.a}$$

$$\frac{\partial \theta_2(X,\tau)}{\partial \tau} = Lu \frac{\partial^2 \theta_2(X,\tau)}{\partial X^2} - LuPn \frac{\partial^2 \theta_1(X,\tau)}{\partial X^2}, \qquad 0 < X < 1, \quad \tau > 0 \tag{11.b}$$

subjected to the initial conditions

$$\theta_1(X,0) = \theta_2(X,0) = 0, \quad 0 \le X \le 1 \tag{11.c,d}$$

and boundary conditions

$$\frac{\partial \theta_1(0,\tau)}{\partial X} = \frac{\partial \theta_2(0,\tau)}{\partial X} = 0, \quad \tau > 0 \tag{11.e,f}$$

$$\frac{\partial \theta_1(1,\tau)}{\partial X} - Bi_q[1-\theta_1(1,\tau)] +$$

$$(1-\varepsilon)KoLuBi_m[1-\theta_2(1,\tau)] + \frac{1}{C_r}\Phi[\theta_1(1,\tau)] = 0, \quad \tau > 0 \qquad (11.g)$$

$$-\frac{\partial \theta_2(1,\tau)}{\partial X} + Pn\frac{\partial \theta_1(1,\tau)}{\partial X} + Bi_m[1-\theta_2(1,\tau)] = 0, \quad \tau > 0 \qquad (11.h)$$

where the function that represents the dimensionless radiation heat flux is given by

$$\Phi[\theta_1(1,\tau)] = -\frac{1}{1-T_0/T_s}\left\{\left(\frac{T_r}{T_s}\right)^4 - \left[\left(1-\frac{T_0}{T_s}\right)\theta_1(1,\tau) + \frac{T_0}{T_s}\right]^4\right\} \qquad (12)$$

The various dimensionless groups employed are defined as:

$\theta_1(X,\tau) = \dfrac{T(x,t)-T_0}{T_s-T_0}$, dimensionless temperature;

$\theta_2(X,\tau) = \dfrac{u_0-u(x,t)}{u_0-u^*}$, dimensionless moisture

$X = \dfrac{x}{\ell}$, dimensionless space coordinate; $\tau = \dfrac{at}{\ell^2}$, dimensionless time;

$Lu = \dfrac{a_m}{a}$, Luikov number

$Pn = \delta \dfrac{T_s - T_0}{u_0 - u^*}$, Possnov number; $Ko = \dfrac{r\,u_0 - u^*}{c\,T_s - T_0}$, Kossovitch number

$Bi_q = \dfrac{h\ell}{k}$, dimensionless heat transfer coefficient; $Bi_m = \dfrac{h_m \ell}{k_m}$, dimensionless mass transfer coefficient

$$C_r = \frac{k}{E\sigma\,\ell T_s^3}, \text{ conduction-to-radiation ratio parameter} \qquad (13.a\text{-}j)$$

The parameter C_r governs the relative importance of the radiative heat exchange at the boundary. Therefore, the larger the value of C_r, less important the effect of radiation. The reference temperature for the radiative heat transfer with the environment, T_r, is not necessarily the same as the temperature of the surrounding air, T_s. Here, in order to reduce the number of parameters to be studied, without loss of generality, we let $T_r = T_s$. Therefore, the function Φ is rewritten as:

$$\Phi[\theta_1(1,\tau)] = -\frac{1}{1 - T_0/T_s}\left\{1 - \left[\left(1 - \frac{T_0}{T_s}\right)\theta_1(1,\tau) + \frac{T_0}{T_s}\right]^4\right\} \qquad (14)$$

The proposed approach was implemented on a Fortran code, and various runs were performed for a rather complete parametric study. The dimensionless times of interest were τ = 0.1, 0.4, and 1.6. The truncation orders were in all cases $N,M \leq 40$, which were observed to be more than sufficient for a relative error target of 10^{-5}. The excellent convergence characteristics of the eigenfunction expansions are illustrated in Tables 3 and 4 for temperature and moisture distributions, respectively.

Table 3: Convergence behavior of temperature expansions.(Lu = 0.4; Pn = 1.0; ε = 0.5; Ko = 1.0; Bi_m=Bi_q = 2.5; C_r = 0.1; T_o/T_s = 0.8)

$\theta_1(X,\tau)$				
τ=0.1				
X/N	5	10	20	30
0.0	0.09005	0.08996	0.08996	0.08996
0.2	0.1155	0.1159	0.1159	0.1159
0.4	0.1987	0.1987	0.1987	0.1987
0.6	0.3547	0.3552	0.3552	0.3552
0.8	0.6130	0.6126	0.6126	0.6126
1.0	0.9712	0.9712	0.9712	0.9712
τ=0.4				
X/N	5	10	20	30
0.0	0.5021	0.5021	0.5021	0.5021
0.2	0.5228	0.5228	0.5229	0.5229
0.4	0.5854	0.5853	0.5854	0.5854
0.6	0.6884	0.6885	0.6885	0.6885
0.8	0.8268	0.8267	0.8267	0.8267
1.0	0.9869	0.9869	0.9869	0.9869
τ=1.6				
X/N	5	10	20	30
0.0	0.8928	0.8928	0.8928	0.8928
0.2	0.8976	0.8976	0.8976	0.8976
0.4	0.9118	0.9118	0.9118	0.9118
0.6	0.9341	0.9341	0.9341	0.9341
0.8	0.9629	0.9629	0.9629	0.9629
1.0	0.9961	0.9961	0.9961	0.9961

Fixed truncation orders were selected, for demonstration purposes N=M=5, 10, 20, 30 and 40, and numerical results presented for τ = 0.1, 0.4, and 1.6. The excellent convergence rates are noticeable even for the smaller values of τ = 0.1, when the temperature field is practically fully converged for $N \leq 10$ and the moisture profile requires $N \cong 20$ terms. For the larger values of τ, $N \cong 5$ provides in most cases four digits of accuracy. The columns for N=40 provide a set of benchmark results for future reference.

The present approach was also employed to validate a previously reported numerical solution [23] of both the linear (C_f=∞) and nonlinear versions of this problem, with good agreement against the Crank-Nicolson finite differences results reported in graphical form in [23]. As shown in Figs 3.a,b, the present procedure with automatic global error control, allows for the safe validation of the previously reported approximate numerical solution. For the uniform mesh size employed in [23], the temperature predictions of that work are slightly less accurate than the moisture results.

Table 4: Convergence behavior of moisture expansions (Lu = 0.4; Pn = 1.0; ε = 0.5; Ko = 1.0; Bi_m=Bi_q = 2.5; C_r = 0.1; T_o/T_s = 0.8)

$\theta_2(X,\tau)$					
τ=0.1					
X/N	5	10	20	30	40
0.0	-0.00823	-0.00935	-0.00930	-0.00930	-0.00930
0.2	-0.02104	-0.02004	-0.01999	-0.01999	-0.01999
0.4	-0.04409	-0.04494	-0.04483	-0.04482	-0.04482
0.6	-0.03471	-0.03228	-0.03203	-0.03201	-0.03201
0.8	0.1597	0.1589	0.1592	0.1592	0.1592
1.0	0.6275	0.6292	0.6294	0.6295	0.6295
τ=0.4					
X/N	5	10	20	30	40
0.0	-0.1225	-0.1223	-0.1223	-0.1223	-0.1223
0.2	-0.09483	-0.09439	-0.09431	-0.09430	-0.09430
0.4	-0.00395	-0.00381	-0.00374	-0.00373	-0.00373
0.6	0.1621	0.1625	0.1626	0.1626	0.1626
0.8	0.4072	0.4070	0.4071	0.4071	0.4071
1.0	0.7062	0.7064	0.7065	0.7065	0.7065
τ=1.6					
X/N	5	10	20	30	40
0.0	0.3142	0.3143	0.3143	0.3143	0.3143
0.2	0.3350	0.3351	0.3351	0.3351	0.3351
0.4	0.3958	0.3958	0.3959	0.3959	0.3959
0.6	0.4922	0.4923	0.4923	0.4923	0.4923
0.8	0.6176	0.6176	0.6176	0.6176	0.6176
1.0	0.7633	0.7633	0.7633	0.7633	0.7633

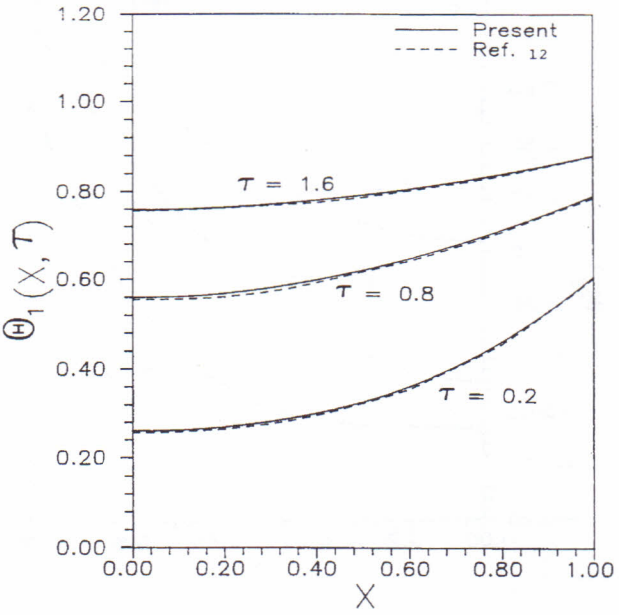

Figure 3.a: Comparison of temperature distributions from present solution and a finite differences solution, Ref. [23]. ($Lu = 0.4$; $Pn = 1.0$, $\varepsilon = 0.5$, $Ko = 1.0$, $Bi_m = 2.5$, $Bi_q = 2.5$, $C_r = 0.1$, $T_o/T_s = 0.2$)

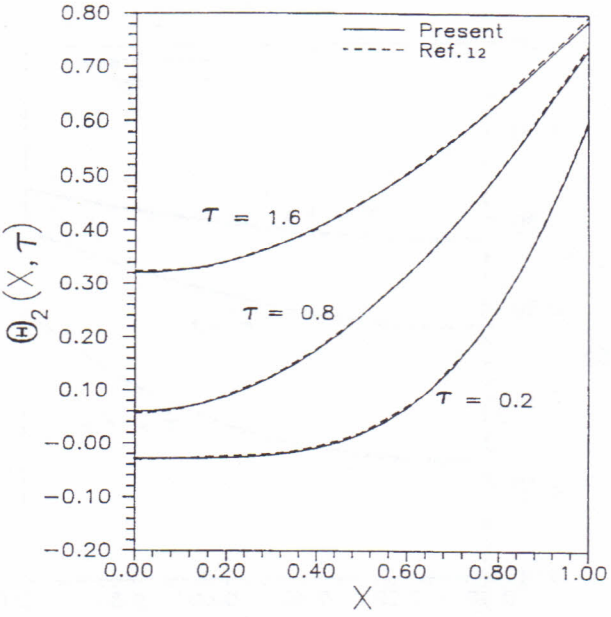

Figure 3.b: Same as above for moisture potential profiles, Ref. [23]

5.3 Convection-Diffusion:- Boundary Layer Formulation

Among the various applications employing the boundary layer equations, already treated through the GITT, we have selected some illustrative results from fairly recent research on mixed convection in channels, both with and without adoption of the Boussinesq approximation [11,25]. Laminar mixed convection of a newtonian fluid developing within vertical parallel plates is considered. The channel is assumed infinite in one transversal direction (z) and semi-infinite in the longitudinal direction (x). The

fluid enters the channel with uniform velocity and temperature profiles, and the channel walls are subjected to a prescribed uniform temperature. The classical Boussinesq approximation is invoked to model the buoyancy effect. Within the range of validity for the boundary layer hypothesis, the vorticity transport and energy equations in the streamfunction-only formulation are written in dimensionless form, respectively, as [25]:

$$\frac{\partial \psi}{\partial y}\frac{\partial^3 \psi}{\partial x \partial y^2} - \frac{\partial \psi}{\partial x}\frac{\partial^3 \psi}{\partial y^3} = \frac{1}{Re}\frac{\partial^4 \psi}{\partial y^4} - \frac{Gr}{Re^2}\frac{\partial \theta}{\partial y}, 0 < y < 1, x > 0 \qquad (15.a)$$

$$\frac{\partial \psi}{\partial y}\frac{\partial \theta}{\partial x} - \frac{\partial \psi}{\partial x}\frac{\partial \theta}{\partial y} = \frac{1}{Pe}\frac{\partial^2 \theta}{\partial y^2}, \qquad 0 < y < 1, x > 0 \qquad (15.b)$$

where the streamfunction is defined in terms of the velocity components in the longitudinal and transversal directions, *x* and *y*, respectively, as:

$$\frac{\partial \psi}{\partial y} = u; \frac{\partial \psi}{\partial x} = -v \qquad (15.c,d)$$

The inlet and boundary conditions, in terms of the streamfunction, are given, respectively, by:

$$\psi(0, y) = y; \qquad \theta(0, y) = 1, \qquad 0 \le y \le 1 \qquad (16.a,b)$$

$$\psi(x,0) = 0; \quad \frac{\partial^2 \psi}{\partial y^2}(x,0) = 0; \quad \frac{\partial \theta}{\partial y}(x,0) = 0, \qquad x > 0 \qquad (16.c\text{-}e)$$

$$\psi(x,1)=1; \qquad \frac{\partial\psi}{\partial y}(x,1)=0; \quad \theta(x,1)=0, \qquad x>0 \tag{16.f-h}$$

The various dimensionless groups are defined as:

$$x=\frac{\bar{x}}{\bar{y}_w}; \quad y=\frac{\bar{y}}{\bar{y}_w}; \quad u=\frac{\bar{u}}{\bar{u}_0}; \quad v=\frac{\bar{v}}{\bar{u}_0}; \tag{17.a-d}$$

$$\theta=\frac{T-T_w}{T_0-T_w}; \quad Re=\frac{\bar{u}_0\bar{y}_w}{\nu}; \quad Pr=\frac{\nu}{\alpha} \quad Pe=Re.Pr. \tag{17.e,g}$$

$$Gr=\frac{g\beta\bar{y}_w^3(T_w-T_0)}{\nu^2}; \tag{17.h}$$

Table 5 presents a convergence analysis of case B in [25] (Gr/Re=131.76; Pr=0.72; parallel-plates channel), for the channel centerline longitudinal velocity component, with a pronounced influence of the buoyancy effect. The first three columns represent the integral transform results for equal truncation orders (*NC=NM*) in the streamfunction and temperature expansions, and are solely intended to build the confidence of the reader in the convergence characteristics of the proposed approach. The actual algorithm works as illustrated in the following column, named as adaptive, and includes the automatically determined truncation orders achieved along the integration path. Finally, the last column, obtained with a truncation order still higher (*NC=NM=80*) than that required for the user requested global accuracy (10^{-4}), serves to confirm the adequacy of the adaptive procedure in providing the four significant digits in the final tabulated solution. As can be noticed, the highest truncation order results agree to within ±1 in the fourth significant digit with the adaptive procedure final results, as expected from the automatic error control scheme of the proposed approach. It is also clear that

even at very low truncation orders (*NC=NM=10*), the integral transform results are already quite representative of the fully converged results, sometimes agreeing to within two, or even three, significant digits.

Some delay on the convergence rates is observable through the region where the natural convection effects are magnified, but not significantly enough to impede full convergence within a practical limit. As expected in eigenfunction expansions-type approaches, convergence improves in regions away from the channel inlet, to finally require few terms as the fully developed region is recovered, when the filtering solution plays an important role in reducing the influence of the equations and boundary conditions source terms.

Table 5: Convergence analysis and adaptive procedure results for the centerline axial velocity component (case B: Gr/Re=131.76 Pr=0.72).

NC/NM X^*	10/10	30/30	60/60	ADAPTIVE NC	NM	$u(X^*,0)$	80/80
0.006	1.0454	1.0497	1.0505	34	57	1.0505	1.0507
0.026	0.60589	0.60782	0.60841	34	50	0.60841	0.60855
0.03	0.52747	0.52898	0.52947	34	33	0.52947	0.52959
0.04	0.39767	0.39815	0.39837	34	33	0.39836	0.39842
0.0432	0.37696	0.37716	0.37729	34	31	0.37728	0.37732
0.117	0.81274	0.81206	0.81191	34	31	0.81191	0.81188
0.3	1.3545	1.3544	1.3544	19	28	1.3544	1.3544
0.6	1.4857	1.4857	1.4857	15	17	1.4857	1.4857
1	1.4993	1.4993	1.4993	10	17	1.4993	1.4993
20	1.5000	1.5000	1.5000	5	17	1.5000	1.5000

The present global error controlled results were then employed in the benchmarking of previously obtained results from purely numerical methods, such as the finite differences implementation of [29] for the same mixed convection problem. Therefore, figures 4.a,b bring a comparison of the fully converged integral transform results and the finite difference results of ref. [29], for the longitudinal velocity component profiles.

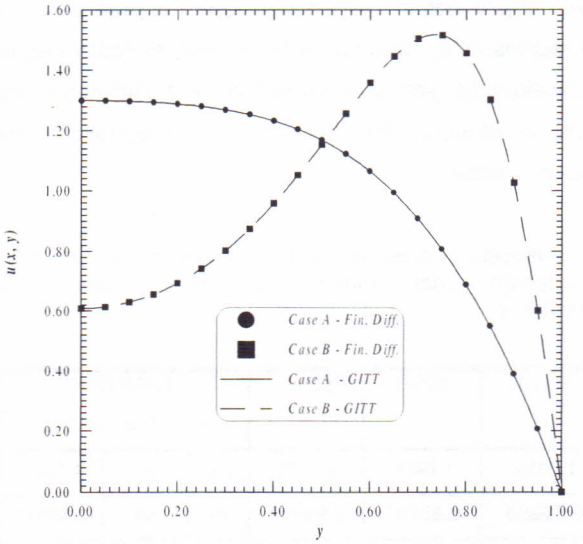

Figure 4.a - Comparison of integral transform and finite differences [29] results for the axial velocity component profile at $X^* = 0.026$ (case A: $Gr/Re = 13.176$ and case B: $Gr/Re = 131.76$).

Figure 4.a is associated with cases A ($Gr/Re = 13.176$) and B ($Gr/Re = 131.76$), at the longitudinal location $X^* = 0.026$, while figure 4.b represents the cases B ($Gr/Re = 131.76$) and D ($Gr/Re = 41.667$), for

$X^* = 0.117$. In both cases, the overall agreement is quite satisfactory, but it is also noticeable that the discrete method results loose adherence, to some extent, in regions of increased velocity gradients as the natural convection effects become more marked, inducing some need for an adaptive remeshing/refinement procedure in such implementation. While the finite differences approach can be significantly improved through such a scheme, it is also true that a price has to be paid on additional development effort, on both the analysis and computational phases of this possible enhanced implementation of a fully discrete method.

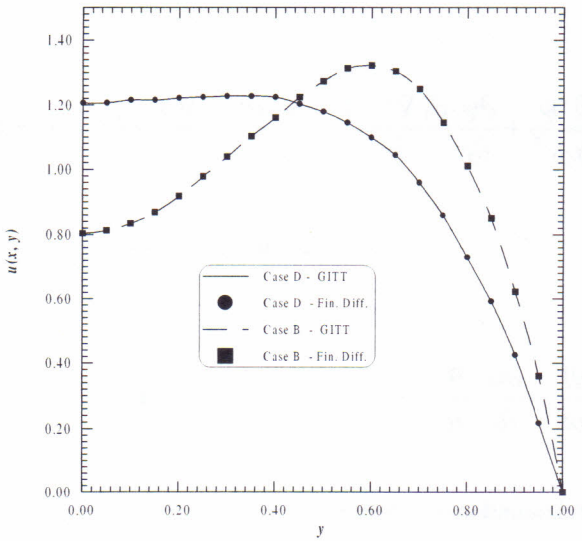

Figure 4.b - Comparison of integral transform and finite differences [29] results for the axial velocity component profile at $X^* = 0.117$ (case B: $Gr/Re = 13.176$ and case D: $Gr/Re = 41.667$).

5.4 Convection-Diffusion:- Navier-Stokes Formulation

We consider a square air-filled enclosure, with differentially heated lateral walls, and insulated top and bottom walls. Buoyancy effects are taken into account through the Boussinesq approximation, under laminar flow regime. Benchmark results for the steady-state situation were established through integral transformation in [35,36], and the transient behavior of the coupled heat and fluid flow phenomena was also investigated [36], for different values of the Rayleigh number, Ra.

The governing equations are the vorticity transport equation in streamfunction-only formulation [30], and the associated energy equation, which in dimensionless form are given by:

$$\frac{\partial^3\psi}{\partial t\partial x^2}+\frac{\partial^3\psi}{\partial t\partial y^2}+\frac{\partial\psi}{\partial y}\frac{\partial(\nabla^2\psi)}{\partial x}-\frac{\partial\psi}{\partial x}\frac{\partial(\nabla^2\psi)}{\partial y}=Pr\,\nabla^4\psi-Pr\,Ra\frac{\partial T}{\partial x}$$

$$0<x<1,\ 0<y<1,\ t>0 \qquad (18.a)$$

$$\frac{\partial T}{\partial t}+\frac{\partial\psi}{\partial y}\frac{\partial T}{\partial x}-\frac{\partial\psi}{\partial x}\frac{\partial T}{\partial y}=\nabla^2 T\ ;\quad 0<x<1,\ 0<y<1,\ t>0 \qquad (18.b)$$

with initial and boundary conditions

$$T(x,y,0)=\psi(x,y,0)=0\ ;\quad 0\le x\le 1\ \ e\ \ 0\le y\le 1 \qquad (18.c,d)$$

$$T=1\ ;\quad \psi=\frac{\partial\psi}{\partial x}=0\ ;\quad x=0 \qquad (18.e\text{-}g)$$

$$T = 0\,; \quad \psi = \frac{\partial \psi}{\partial x} = 0\,; \qquad x = 1 \tag{18.h-j}$$

$$\frac{\partial T}{\partial y} = 0\,; \quad \psi = \frac{\partial \psi}{\partial y} = 0\,; \qquad y = 0 \tag{18.k-m}$$

$$\frac{\partial T}{\partial y} = 0\,; \quad \psi = \frac{\partial \psi}{\partial y} = 0\,; \qquad y = 1 \tag{18.n-p}$$

where the Rayleigh number is defined as:

$$Ra = \frac{g\,\beta\,(T_h - T_c)\,L^3}{\alpha\,\nu} \tag{19}$$

and L is the enclosure height and length, while T_h and T_c are the hot and cold wall temperatures, respectively.

Table 6 illustrates some of the benchmark results obtained for the steady-state solution, in this case for $Ra=10^6$, compared against previously reported purely numerical solutions, as detailed in [35]. The agreement is indeed excellent, reconfirming some of the most recent and careful benchmarking efforts available in the literature, even for the slower converging Nusselt number expansions.

Table 6 - Comparison of steady-state benchmark results for natural convection in a square cavity ($Ra = 10^6$, $Pr=0.71$).

	GITT	Vahl Davis[37]	Saitoh & Hirose [38]	Hortmann et al. [39]	Lé Queré [40]
$\lvert\psi_{MED}\rvert$	16.39	16.32	16.379	NA	16.386
$\lvert\psi_{MAX}\rvert$	16.81	16.750	NA	NA	16.811
x,y	0.151, 0.547	0.151, 0.547			0.150, 0.547
u_{MAX}	64.83	64.63	64.886	64.8367	64.83
y	0.850	0.850	0.8505	0.85036	0.850
v_{MAX}	220.6	219.36	220.47	220.461	220.6
x	0.0379	0.0379	0.03783	0.03887	0.038
$\overline{Nu}$	8.825	8.800	8.7956	8.82513	8.825
$Nu_{1/2}$	8.825	8.799	8.7989	8.82513	8.825
Nu_0	8.826	8.817	8.8487	8.82513	8.825
Nu_{MAX}	17.54	17.925	17.140	17.536	17.536
y	0.0390	00378	0.0473	0.03902	0.039
Nu_{MIN}	0.9794	0.989	1.015	NA	0.9795
y	1	1	1		1

NA - Not Available

Figures 5.a,b show a comparison of the transient integral transform results against a finite elements simulation [41] at different dimensionless times for, respectively, temperature and vertical velocity component distributions along the longitudinal coordinate, with $Ra = 10^5$.

Again, the agreement is quite reasonable to the graph scale within the transient region, with some more noticeable deviations as the steady-state is approached, due to some error propagation effect in the purely numerical solution.

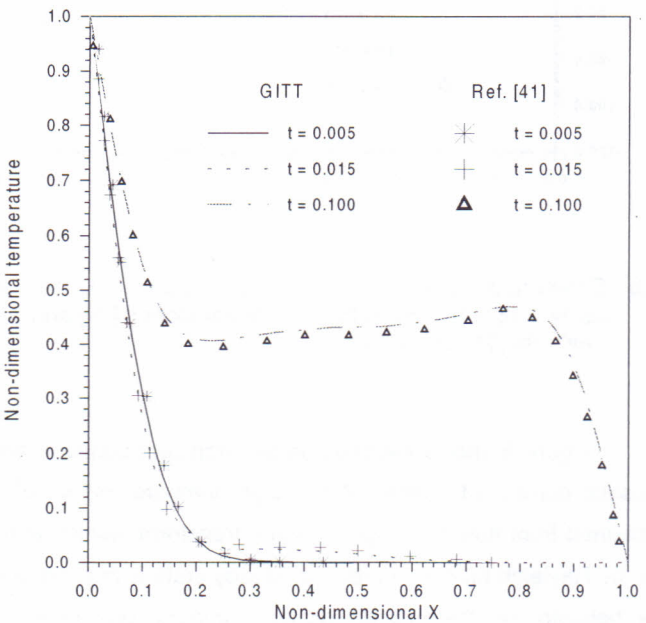

Figure 5.a - Comparison of transient temperature distributions at the cavity midplane (y=1/2) by integral transforms [36] and finite elements [41], ($Ra = 10^5$).

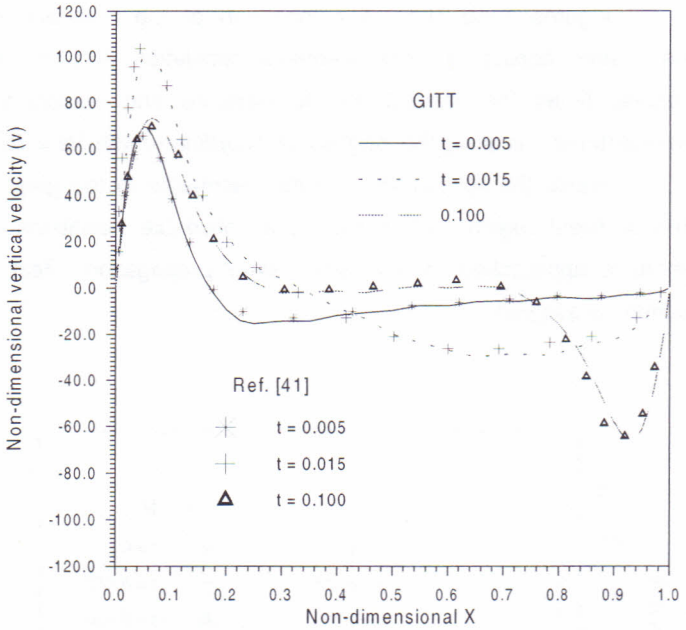

Figure 5.b - Comparison of transient vertical velocity component (v) at the cavity midplane (y=1/2) by integral transforms [36] and finite elements [41], ($Ra = 10^5$).

Figure 6 shows the comparative transient behavior among the overall Nusselt numbers for different Rayleigh numbers, $Ra = 10^3$, 10^4 and 10^5, as obtained from fully converged integral transform results, to the graph scale. As the Rayleigh number increases, steady-state is reached after some oscillatory behavior on the overall Nusselt numbers, due to internal flow waves developed at early transient stage. As Ra is further increased, this phenomena leads to flow instabilities that restrict the system in reaching a fully steady pattern.

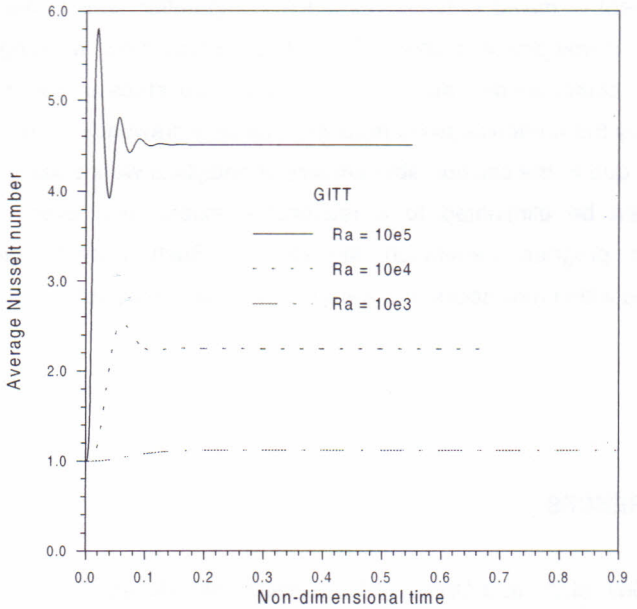

Figure 6 - Transient behavior of the overall average Nusselt number in a square cavity for different Rayleigh numbers ($Ra = 10^3$, 10^4 and 10^5).

Algorithm optimization schemes should then allow for the employment of the integral transform approach in the analysis of unstable heat and fluid flow phenomena, with the quite desirable automatic error control feature, essential for the discrimination between numerical and physical oscillations in the final solution patterns.

6: CONCLUSIONS

Future research needs are very closely associated with the development of mixed symbolic-numerical computation, which offers a very adequate development platform for hybrid approaches, allowing for the automatic computer derivation of all the analytical steps in the procedure, followed by the numerical tasks required. The only drawback in such class of methods, due to the considerable amount of analytical work usually required, would then be eliminated to a reasonable extent, and even, allow for automatic program generation strategies. Such aspects are better envisioned within new books that were recently made available [11,42].

7 REFERENCES

1. Mikhailov, M.D. and Özisik, M.N., *Unified Analysis and Solutions of Heat and Mass Diffusion*, John Wiley, New York, 1984; also, Dover Publications, 1994.

2. Cotta, R.M., *Integral Transforms in Computational Heat and Fluid Flow*, CRC Press, Boca Raton, FL, 1993.

3. Cotta, R.M., Benchmark Results in Computational Heat and Fluid Flow: - The Integral Transform Method, *Int J. Heat & Mass Transfer* (Invited Paper), **37**, Suppl. 1, pp.381-394, 1994.

4. Cotta, R.M., The Integral Transform Method in Computational Heat and Fluid Flow, Special Keynote Lecture, Proc. of the *10th Int. Heat Transfer Conf.*, Brighton, UK, SK-3, V. 1, pp. 43-60, August 1994.

5. Mikhailov, M.D. and Cotta, R.M., Unified Integral Transform Method, *J. Braz. Assoc. Mech. Sciences* (Invited Paper), **12**, no. 3, pp.301-310, 1990.

6. Cotta, R.M. and Mikhailov, M.D., The Integral Transform Method, *Appl. Math. Modelling*, **17**, pp.156-161, 1993.

7. Cotta, R.M., Hybrid Numerical-Analytical Approach to Nonlinear Diffusion Problems, *Num. Heat Transfer, Part B - Fundamentals*, **127**, pp. 217-226, 1990.

8. Serfaty, R. and Cotta, R.M., Hybrid Analysis of Transient Nonlinear Convection-Diffusion Problems, *Int. J. Num. Meth. Heat & Fluid Flow*, **2**, pp.55-62, 1992.

9. *IMSL Library*, MATH/LIB, Houston, TX, 1987.

10. Cotta, R.M. and Mikhailov, M.D., *Heat Conduction:- Lumped Analysis, Integral Transforms, Symbolic Computation*, John Wiley, New York, 1997.

11. Cotta, R.M. (ed.), *The Integral Transform Method in Thermal and Fluids Sciences and Engineering*, Begell House, New York, 1998.

12. R.M. Cotta and R. Ramos, "Error Analysis and Improved Formulations for Extended Surfaces", Proc. of the *NATO Advanced Study Institute on Cooling of Electronic Systems*, NATO ASI Series E: Applied Sciences, **258**, pp. 753-787, Turkey, June/July 1993.

13. J.B. Aparecido, R.M. Cotta, and M.N. Ozisik, "Analytical Solutions to Two-Dimensional Diffusion Type Problems in Irregular Geometries", *J. Franklin Institute*, **326**, 421-434 (1989).

14. J.B. Aparecido and R.M. Cotta, "Laminar Flow Inside Hexagonal Ducts", *Computational Mechanics*, **6**, 93-100 (1990).

15. J.B. Aparecido and R.M. Cotta, "Analytical Solution to Parabolic Multidimensional Diffusion Problems Within Irregularly Shaped Domains", Proc. of the *Int. Conf. on Advanced Computational Methods in Heat Transfer*, **1**, pp. 27-38, Southampton, UK, July 1990.

16. J.B. Aparecido and R.M. Cotta, "Laminar Thermally Developing Flow Inside Right Triangular Ducts", *Appl. Scientific Research*, **49**, 355-368 (1992).

17. A. Aziz and H. Nguyen, "Two-Dimensional Effects in a Triangular Convecting Fin", *J. Thermophysics & Heat Transfer*, **6**, no. 1, 165-167 (1992).

18. B.T.F. Chung, M.H. Abdalla, and F. Liu, "Optimization of Convective Longitudinal Fins of Trapezoidal Profile", *Chem. Eng. Comm.*, **80**, 211-223 (1989).

19. A.V. Luikov, "Heat and Mass Transfer in Capillary Porous Bodies", *Advances in Heat Transfer*, **1**, pp. 123-184, 1964.

20. J.W. Ribeiro, R.M. Cotta, and M.D. Mikhailov, "Integral Transform Solution of Luikov's Equations for Heat and Mass Transfer in Capillary Porous Media", *Int. J. Heat & Mass Transfer*, **36**, no. 18, 4467-4475 (1993).

21. J.W. Ribeiro and R.M. Cotta, "Numerical-Analytical Study of Nonlinear Drying Problems with Radiative Boundaries", Proc. of the 6^{th} *Int. Symp. Transport Phenomena: Thermal Engineering*, **1**, pp. 209-214, Seoul, Korea, May 1993.

22. J.W. Ribeiro and R.M. Cotta, "On the Solution of Nonlinear Drying Problems in Capillary Porous Media Through Integral Transformation of Luikov Equations", *Int. J. Num. Meth. Eng.*, **38**, 1001-1020 (1995).

23. P.D.C. Lobo, "*On the Solution of a Nonlinear Combined Heat and Mass Transfer Problem*", Ph.D. Dissertation, North Carolina State University, USA, (1988).

24. J.B.F. Duarte, J.W. Ribeiro, and R.M. Cotta, "An Integral Transform Solution of Two-Dimensional Drying of Moist Porous Media", Proc. of the *3rd Int. Congress on Industrial and Applied Mathematics, ICIAM 95,* Hamburg, Germany, July 1995.

25. Figueira da Silva, E. and Cotta, R.M., Mixed Convection Within Vertical Parallel-plates:- Hybrid Solution by Integral Transforms, *Num. Heat Transfer, part A – Applications*, **33**, pp.85-106, 1998.

26. R.M. Cotta and T.M.B. Carvalho, Hybrid Analysis of Boundary Layer Equations for Internal Flow Problems, *Proc. of the 7th. Int. Conf. on Num. Meth. in Laminar & Turbulent Flow*, Part 1, pp.106-115, Stanford, CA, July 1991.

27. T.M.B. Carvalho, R.M. Cotta, and M.D. Mikhailov, Flow Development in The Entrance Region of Ducts., *Comm. Num. Meth. Eng.*, **9**, pp.503-509, 1993.

28. H.A. Machado and R.M. Cotta, Integral Transform Method for Boundary Layer Equations in Simultaneous Heat and Fluid Flow Problems, *Int. J. Num. Meth. Heat & Fluid Flow*, **5**, pp. 225-237, 1995.

29. S. Habchi and S. Acharya, Laminar Mixed Convection in a Symmetrically or Asymmetrically Heated Vertical Channel, *Numerical Heat Transfer*, **9**, pp.605-618, 1986.

30. J.S. Perez Guerrero and R.M. Cotta, Integral Transform Method for Navier-Stokes Equations in Streamfunction-Only Formulation, *Int. J. Num. Meth. Fluids*, **15**, pp.399-409, 1992.

31. R.M. Cotta, J.S. Perez Guerrero, and F. Scofano Neto, Hybrid Solution of the Incompressible Navier-Stokes Equations via Integral Transformation, *Proc. of the 2nd. Int. Conf. Adv. Comp. Meth. in Heat Transfer, "Heat Transfer 92"*, **1**, pp.735-750, Milan, Italy, July 1992.

32. C. Baohua and R.M. Cotta, Integral Transform Analysis of Natural Convection in Porous Enclosures, *Int. J. Num. Meth. in Fluids*, **17**, pp.787-801, 1993.

33. J.S. Perez Guerrero, R.M. Cotta, and F. Scofano Neto, Integral Transformation of Navier-Stokes Equations for Incompressible Laminar Flow in Channels, *Proc. of the 8th. Int. Conf. Num. Meth. in Laminar & Turbulent Flow*, **2**, pp.1195-1206, Swansea, UK, July 1993.

34. J.S. Perez Guerrero and R.M. Cotta, Integral Transform Solution of Developing Laminar Duct Flow in Navier-Stokes Formulation, *Int. J. Num. Meth. in Fluids*, **20**, pp.1203-1213, 1995.

35. Leal, M.A., J.S. Pérez Guerrero and R.M. Cotta, "Natural Convection Inside Two-Dimensional Cavities: - The Integral Transform Method", *Comm. Num Meth. Eng.*, **15**, pp., 1999.

36. Leal, M.A. and R.M.Cotta, "Steady and Transient Integral Transform Solutions of Natural Convection in Enclosures", *Proc. of the ICHMT Int. Symp. on Computational Heat Transfer*, Turkey, May 1997.

37. de Vahl Davis, G., "Natural Convection of Air in a Square Cavity: a Bench Mark Numerical Solution", *Int. J. Num. Meth. in Fluids*, **3**, pp. 249-264, 1983.

38. Saitoh, T. and K. Hirose, "High-accuracy Bench Mark Solutions to Natural Convection in a Square Cavity", *Computational Mechanics*, **4**, pp. 417-427, 1989.

39. Hortmann, M., M. Peric and G. Scheuerer, "Finite Volume Multigrid Prediction of Laminar Natural Convection: Bench-Mark Solutions", *Int. J. Num. Meth. in Fluids*, **11**, pp. 189-207, 1990.

40. Le Quéré, P., "Accurate Solutions to the Square Thermally Driven Cavity at High Rayleigh Number", *Computers & Fluids*, **20**, n° 1, pp. 29-41, 1991.

41. Sai, B.V.K.S., K.N. Seetharamu, and P.A.A. Narayana, "Solution of Transient Laminar Natural Convection in a Square Cavity by an Explicit Finite Element Scheme", *Num. Heat Transfer, Part A*, **25**, pp. 593-609, 1994.

42. Mikhailov, M.D. and R.M. Cotta, *Integral Transform Method with Mathematica*, in preparation.